



**HAL**  
open science

## Cation Alloying Delocalizes Polarons in Lead-halide Perovskites

Liujiang Zhou, Claudine Katan, Wanyi Nie, Hsinshan Tsai, Laurent Pedesseau, Jared J Crochet, Jacky Even, Aditya D Mohite, Sergei Tretiak, Amanda J Neukirch

► **To cite this version:**

Liujiang Zhou, Claudine Katan, Wanyi Nie, Hsinshan Tsai, Laurent Pedesseau, et al.. Cation Alloying Delocalizes Polarons in Lead-halide Perovskites. *Journal of Physical Chemistry Letters*, 2019, 10 (13), pp.3516-3524. 10.1021/acs.jpcllett.9b01077 . hal-02151543

**HAL Id: hal-02151543**

**<https://hal.science/hal-02151543v1>**

Submitted on 18 Nov 2019

**HAL** is a multi-disciplinary open access archive for the deposit and dissemination of scientific research documents, whether they are published or not. The documents may come from teaching and research institutions in France or abroad, or from public or private research centers.

L'archive ouverte pluridisciplinaire **HAL**, est destinée au dépôt et à la diffusion de documents scientifiques de niveau recherche, publiés ou non, émanant des établissements d'enseignement et de recherche français ou étrangers, des laboratoires publics ou privés.

# Cation Alloying Delocalizes Polarons in Lead-halide Perovskites

*Liujiang Zhou<sup>\*†‡</sup>, Claudine Katan<sup>†</sup>, Wanyi Nie<sup>§</sup>, Hsinhan Tsai<sup>§</sup>, Laurent Pedesseau<sup>//</sup>, Jared J. Crochet<sup>⊥</sup>, Jacky Even<sup>//</sup>, Aditya D. Mohite<sup>#</sup>, Sergei Tretiak<sup>‡</sup>, and Amanda J. Neukirch<sup>‡\*</sup>.*

<sup>†</sup> Institute of Fundamental and Frontier Sciences, University of Electronic Science and Technology of China, Chengdu 610054, P. R. China

<sup>‡</sup> Theoretical Physics and Chemistry of Materials, Los Alamos National Laboratory, Los Alamos, New Mexico 87545, USA

<sup>†</sup> Univ Rennes, ENSCR, INSA Rennes, CNRS, ISCR - UMR 6226, F-35000 Rennes, France

<sup>§</sup> Materials Physics and Application, Los Alamos National Laboratory, Los Alamos, New Mexico 87545, USA

<sup>//</sup> Physical Chemistry and Applied Spectroscopy Division, Los Alamos National Laboratory, Los Alamos, New Mexico 87545, USA

<sup>⊥</sup> Univ Rennes, INSA Rennes, CNRS, Institut FOTON - UMR 6082, F-35000 Rennes, France

<sup>#</sup> Department of Chemical and Biomolecular Engineering, Rice University, Houston, Texas 77006, USA

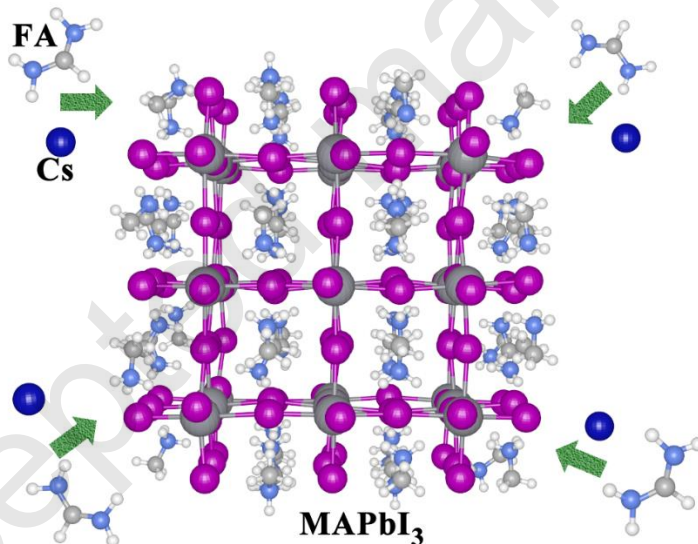
\* Email: liujiang86@gmail.com; ajneukirch@lanl.gov

## **ABSTRACT**

Recently, mixed-cation perovskites have promised enhanced performances concerning stability and efficiency in optoelectronic devices. Here, we report a systematic study on the effects of cation alloying on polaronic properties in cation-alloyed perovskites using first principle

calculations. We find that cation alloying significantly reduces the polaron binding energies for both electrons and holes compared to pure methylammonium lead iodide (MAPbI<sub>3</sub>). This is rationalized in terms of crystal symmetry reduction that causes polarons to be more delocalized. Electron polarons undergo large Jahn-Teller distortions (~15–30%) while hole polarons tend to shrink lattice by ~5%. Such different lattice distortion footprints could be utilized to distinguish the type of polarons. Finally, our simulations show that a Cs, formamidinium (FA) and MA mixture can effectively minimize polaron binding energy while weakly affecting band gap, in a good agreement with experimental findings. These modeling results can guide future development of halide perovskite materials compositions for optoelectronic applications.

#### TOC GRAPHIC



Three-dimensional lead-halide perovskites with general formula APbX<sub>3</sub> (where A is a monovalent cation and X = I, Br, or Cl) are comprised of earth-abundant elements and are solution processable. These materials were shown promise for various optoelectronic applications while retaining low cost.<sup>1,2</sup> The prototypical halide perovskite, MAPbI<sub>3</sub>, with a band gap of 1.6 eV,<sup>3</sup> has been successfully utilized as an excellent active material for light harvesting in solar cells with

outstanding power conversion efficiency approaching 21%.<sup>4</sup> In fact, solution-processed halide perovskites (HPs) are favorable candidates for a diverse range of applications including photovoltaics, light-emitting diodes,<sup>5,6</sup> hydrogen generation,<sup>7</sup> X-ray and gamma-ray detection,<sup>8,9</sup> spintronics<sup>10</sup> and sensors.<sup>11</sup> The superb performances of halide perovskites are due to unique photophysical traits, including low carrier effective masses, low electron-hole recombination rates, ambipolar charge transport, high extinction coefficients, and long charge carrier diffusion lengths.<sup>12–14</sup>

Despite these initial demonstrations, the most significant barrier in the progress towards halide perovskite device commercialization is the lack of stability to temperature, oxygen, humidity, and exposure to light.<sup>15–17</sup> Hybrid perovskites are prone to chemical reactions, phase transformations, phase segregation, and other degradation processes under ambient conditions. Numerous strategies, including reducing structural dimensionality,<sup>18,19</sup> chemical make-up,<sup>20,21</sup> anti-solvent additive deposition,<sup>22</sup> and defect creation,<sup>23</sup> have been applied to the original MAPbI<sub>3</sub> structure in order to achieve a more stable while efficient solar cell material.<sup>24,25</sup> For example, when making A-site substitutions to the lead-halide perovskites, various improvements are found. The FAPbI<sub>3</sub> perovskite has an advantageous red-shift in bandgap and is less susceptible to thermal degradation compared to its MA equivalent.<sup>25,26</sup> However, it lacks structural stability and its photoactive  $\alpha$ -phase (“black phase”) is stable at elevated temperatures (>60 °C).<sup>27</sup> At room temperature FAPbI<sub>3</sub> tends to transform into the non-perovskite  $\delta$ -phase (“yellow phase”).<sup>27</sup> One of the main reasons for decomposition of MA and FA perovskites is the high volatility of the organic cations.<sup>28</sup> Therefore the all inorganic alternative, CsPbI<sub>3</sub> has drawn a lot of consideration.<sup>25,27,29–31</sup> Cs salts are less volatile than their organic counterparts, and exhibit excellent thermal stability up to temperatures as high as 300 °C.<sup>29,31–33</sup> Unfortunately, in addition to having a larger band gap,

CsPbI<sub>3</sub> also suffers for the poor stability of its  $\alpha$ -phase and at room temperature tends to transform into another non-perovskite yellow  $\delta$ -phase.<sup>34</sup> In absence of pure material exhibiting optimal optoelectronic properties and thermodynamic stability, alloyed materials may offer further structural optimizations. It has been widely demonstrated that double and/or triple cations perovskite compositions hold out the best solar cell performances. Adding small amounts of MA and Cs to FA perovskites induces crystallization into the photoactive perovskite phase and results in a composition that is more thermally and structurally stable than any of the pure systems.<sup>25,35-42</sup>

Besides, MAPbI<sub>3</sub> also suffers from the reversible photo-degradation in experiment<sup>43</sup> that was attributed to light-activated metastable trap states of atomistic origin.<sup>43,44</sup> Experimental and theoretical characterizations suggest that localized charged states strongly couple to local structural lattice distortions and methyl ammonium (MA) quasistatic configurations. These small polarons seed the creation of macroscopic charged domains prohibiting efficient charge extraction. Since these initial studies, there has been additional evidence that polarons play a role in the charge carrier behavior in perovskite materials.<sup>45-50</sup> In the process of thermalization, the polaron phonon can reach equilibration by transferring thermal energy to surrounding lattice, giving rise to a cooled charge carrier.<sup>51</sup> Small polaron are believed to be minority carriers that can lead to shifts in the near-infrared absorption edge, local structural distortions, as well as steep temperature dependent photo-degradation in perovskite materials.<sup>43</sup> In order to reduce photo-degradation and enhance the carriers' mobility and boost photocurrent in perovskite materials, it is therefore highly desirable to find a way to control the dressed quasiparticles in terms of spatial delocalization and the binding energy to the lattice degrees of freedom. Indeed, the formation of small polarons in MAPbI<sub>3</sub> was initially traced to cooperative MA<sup>+</sup> rotation and volumetric lattice strain. This interpretation was consistent with lower polaron binding energies in CsPbI<sub>3</sub> for both electrons and holes, and led to

the hypothesis that FAPbI<sub>3</sub> would be the best pure material to alleviate the photodegradation.<sup>44</sup> Alloying Cs, FA, and MA shall inhibit both concerted dipolar rotations and charge induced volumetric strain and thus has the potential to further affect the small polarons spatial distribution and reduce its binding energy.<sup>40,44</sup> Notice that large polaron formation is also affected by alloying, leading to a slight enhancement of large polaron stabilization, due to Cs apolar character, not screening added charges.<sup>51</sup>

In this letter, we utilize *ab initio* calculations to systematically investigate polaronic properties in a variety of mixed-cation hybrid perovskites. With the respect to Goldschmidt tolerance factor, mixtures of the three cations lead on the average to suitable structural stability tolerances. An additional advantage of alloying is the local symmetry breaking that prevents cooperative charge trapping through “concerted” cation re-configurations. Mixed triple cation could form perovskite with almost constant band gaps. Our modeling shows that cation alloying significantly reduces the polaron binding energies for both electrons and holes compared to that in pure MAPbI<sub>3</sub>. This can be traced to a pre-breaking of the crystal symmetry. Electron polarons undergo a Jahn-Teller (JT) distortions with the central apical bonds stretching 15-30% from their neutral geometry and the equatorial bonds remaining nearly the same. Hole polarons get the central octahedrons contracted uniformly by about 5%. Thus, the cation-mixing seems to effectively control both the structural and electronic properties so as to improve materials performance of halide perovskites.

Materials with ABX<sub>3</sub> composition make different crystal structures contingent upon the size and interaction of the A cation and the corner-sharing BX<sub>6</sub> octahedra. The Goldschmidt tolerance (t) is a reliable empirical index to predict what structure is preferentially formed.<sup>52</sup> The

Goldschmidt tolerance factor is calculated from the ionic radius of the atoms using the following expression:

$$t = \frac{r_A + r_X}{\sqrt{2}(r_B + r_X)} \quad (1)$$

Where  $r_A$  is the radius of the A cation,  $r_B$  is the radius of the B cation and  $r_X$  is the radius of the anion. In general, corner-sharing perovskites can be formed in the range of  $0.8 < t < 1.0$ .<sup>53,54</sup> Using the Pauling radii<sup>55</sup> for  $\text{Cs}^+ = 1.69$ ,  $\text{Pb}^{2+} = 1.22$ , and  $\text{I}^- = 2.16$  and reasonable values for  $\text{MA}^+ = 2.17$  and  $\text{FA}^+ = 2.56$ ,<sup>56</sup> we get that the tolerance factor for  $\text{CsPbI}_3$  is 0.805,  $\text{MAPbI}_3$  is 0.906, and  $\text{FAPbI}_3$  is 0.987. To achieve the ideal black perovskite phase, tolerance factor  $t$  must be limited by the range of 0.9–1.0.  $\text{CsPbI}_3$ , with  $t = 0.805$ , is too small to sustain the large  $\text{PbI}$  framework and induces large octahedral tilting accompanied with local lattice distortions.<sup>57</sup> This observation is in line with the tremendous difficulty of fabricating stable  $\text{CsPbI}_3$  perovskites at room temperature. With a tolerance factor close to 1, FA should adopt a nearly cubic lattice. However, due to the disordered states of FA cations in the cuboctahedral cages formed with 12 nearest-neighbor I atoms,<sup>58</sup> the asymmetrical FA ions reside off-center in the  $\text{PbI}_6$  octahedron causing the formation of a hexagonal non-perovskite structure.<sup>59</sup> This suggests design the alloyed perovskites containing a suitable mixing of the three cations, which yields an optimal tolerance factor and improvement of the stability of the perovskite and photo-active phase, as already confirmed in experiments.<sup>39,40</sup>

The three pure perovskites,  $\text{APbI}_3$  ( $A = \text{Cs}, \text{MA}, \text{FA}$ ), have indeed optical absorption onsets at  $\sim 1.73$  (black phase),<sup>60</sup> 1.51 (Tetragonal),<sup>58</sup> and 1.43 (cubic)<sup>58</sup> eV, respectively. The band gap redshift from Cs to MA to FA is associated to decreasing octahedral tilting with increasing cation size.<sup>56,61</sup>  $\text{MAPbI}_3$  doping with Cs and FA is not expected to significantly change octahedral tilting and is anticipated to marginally change the band gap.<sup>62,63</sup> At the HSE+SOC level of theory, pure periodic  $\text{MAPbI}_3$  has a band gap of 1.01–1.17 eV.<sup>44</sup> At this same level of theory, we built a periodic

tri-cation model of  $\text{FA}_{0.688}\text{MA}_{0.25}\text{Cs}_{0.063}\text{PbI}_3$  in tetragonal phase containing 185 atoms to mimic the stoichiometric ratio ( $\text{FA}_{0.7}\text{MA}_{0.25}\text{Cs}_{0.05}\text{PbI}_3$ ) explored in experiment.<sup>40</sup> We find this mixed-cation system has a band gap of 1.18 eV. This indicates that Cs and FA co-doping does not heavily influence the band gaps of materials.

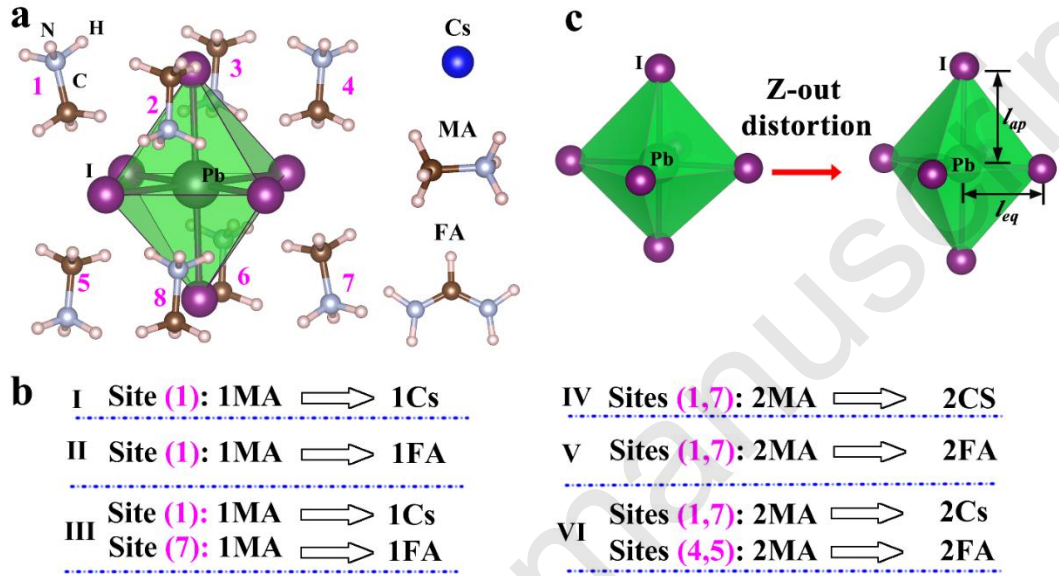


Figure 1: (a) Schematic diagram of a  $\text{PbI}_6$  octahedron and the eight surrounding MA molecules. (b) Six substitution models are derived from the basic  $\text{MAPbI}_3$  cluster with a stoichiometry of  $\text{A}_{54}\text{Pb}_{27}\text{I}_{108}$ , where A is a mixture of the three cations. These models are denoted as Cs- $\text{MAPbI}_3$  (I), FA- $\text{MAPbI}_3$  (II), CsFA- $\text{MAPbI}_3$  (III), 2Cs- $\text{MAPbI}_3$  (IV), 2FA- $\text{MAPbI}_3$  (V), and 2(CsFA)- $\text{MAPbI}_3$  clusters (VI). The Cs and FA substitutions are considered along a diagonal around the central Pb in order to minimize the net dipole moment. The pink numbers are denoted to mark the sites where the substitutions are performed. (c) Schematic diagram of Jahn-Teller (JT) distortions. The equatorial ( $l_{eq}$ ) and apical ( $l_{ap}$ ) bond lengths are also marked.

In order to describe the substitution effect on the charge species (i.e., polaron size and its binding energy), we subsequently constructed a series of cation-mixed isolated clusters (Figure 1a) based on a pure  $\text{MAPbI}_3$  cluster where the MA cations are arranged in an antiferroelectric order



along the diagonal direction (Figure 1a,b). Assessment of polaronic effects assumes optimization of geometries of neutral and charged clusters followed by calculations of energies at these configurations<sup>44,64,65</sup> (see SI and discussion below). These simulations were carried out using Gaussian 16 software package<sup>66</sup> under the hybrid exchange-correlation CAM-B3LYP functional<sup>67</sup> in a polarizable solvent (see computational details in Supplementary Information). Due to the size of the system, the use of a hybrid functional, and the intentional use of a local basis set, it was not possible to include the spin orbit coupling (SOC) effects to these calculations. This limitation does add a few caveats to our results. The electron reorganization/polaron binding energies are overestimated because of the lack of inclusion of SOC. Previously, we have also observed that due to the degeneracy at the bottom of the conduction band in the absence of SOC, the estimated Jahn-Teller distortions and displacements are larger than those observed in experiment.<sup>68</sup> In spite of these limitations, general trends across the materials series are predicted correctly.

One important aspect of carrier self-trapping and spatial localization is symmetry breaking that may show itself in the activation of normally forbidden infrared modes.<sup>64,65</sup> Electron coupling to acoustic or polar optical phonons leads to different polaronic species in semiconductor lattices with well-defined point group symmetries.<sup>44</sup> Empirical Hamiltonians, like Holstein's,<sup>65</sup> are built to introduce a non-linearity into Schrodinger's equation and provoke a bifurcation. A purely small polaron scenario related to totally symmetric local strain was presented in our previous manuscript.<sup>44</sup> The JT distortions in HP materials is important in small polaron formation of electrons and is discussed in this manuscript and other previous manuscripts.<sup>68,69</sup> The JT distortion is intimately linked to electronic degrees of freedom and is important signature of small polaron formation.<sup>69,70</sup> Consequently, it manifests in removing an electronic degeneracy, opening a band gap and favoring a particular electronic state.

**Table 1. Change in Pb-I Equatorial ( $l_{eq}$ ) and Apical Bond ( $l_{ap}$ ) Lengths (in Å) of the central Octahedron as defined in Figure 1c, as well as their standard deviations ( $\sigma$ ) in mixed systems.**

Change in Pb-I bond length (%)			
	Electron		Hole
	$l_{eq}$	$l_{ap}$	Both
<b>CsPbI<sub>3</sub></b>	2	32	-5
<b>MAPbI<sub>3</sub></b>	2	25	-5
<b>FAPbI<sub>3</sub></b>	-2	23	-6
<b>Model-I</b>	2	17	-5
<b>Model-II</b>	2	15	-5
<b>Model-III</b>	3	14	-5
<b>Model-IV</b>	2	16	-5
<b>Model-V</b>	2	15	-5
<b>Model-VI</b>	2	17	-5
<b><math>\sigma</math></b>	0.37	1.11	0

Table 1 summarizes calculated changes in bond lengths, and energies between neutral and charged cluster obtained by comparing their respective optimal geometries. As with previous results,<sup>69</sup> we find that the hole polaron bond lengths universally shrink by about 5% in all directions (Table 1). For the electron polaron in all the materials studied, the bond lengths of the four equatorial Pb-I bonds ( $l_{eq}$ ) in the central octahedron remain almost unchanged. In contrast, the apical Pb-I bond lengths ( $l_{ap}$ ) in the central octahedron increase by at least 23% for the pure materials with Cs (32%) > MA(25%) > FA (23%), reflecting the order of inherent symmetry. Markedly, the effect is notably reduced to about 15% for mixed cation materials with a standard deviation of 1.11. Thus, while the local lattice symmetry is also broken by the formation of electron polarons in alloyed systems, it is suggestive that they are less likely to be observed in these systems due to smaller geometrical changes.

**Table 2: Cavity Volumes (in Å<sup>3</sup>), Reorganization Energies ( $\lambda$ , meV) and Polaron Binding Energies ( $E_{\text{pol}}$ , meV) calculated for CsPbI<sub>3</sub>, MAPbI<sub>3</sub>, FAPbI<sub>3</sub>, and Mixed-cation Systems**

Models	Volume	Electron			Hole		
		$\lambda_1$	$\lambda_2$	$\lambda, E_{\text{pol}}$	$\lambda_1$	$\lambda_2$	$\lambda, E_{\text{pol}}$
<b>CsPbI<sub>3</sub></b>	<b>9993</b>	724	918	1642, 821 <sup>B</sup>	365	274	639, 320 <sup>C</sup>
<b>MAPbI<sub>3</sub></b>	<b>10350</b>	510	1377	1887, 944 <sup>B</sup>	528	578	1106, 553 <sup>A</sup>
<b>FAPbI<sub>3</sub></b>	<b>10708</b>	536	723	1259, 630 <sup>B</sup>	310	506	816, 408 <sup>B</sup>
<b>Model-I</b>	<b>10322</b>	525	677	1202, 601 <sup>B</sup>	275	399	674, 337 <sup>B</sup>
<b>Model-II</b>	<b>10350</b>	545	621	1166, 583 <sup>B</sup>	337	238	575, 288 <sup>C</sup>
<b>Model-III</b>	<b>10335</b>	541	572	1113, 557 <sup>A</sup>	365	289	654, 327 <sup>C</sup>
<b>Model-IV</b>	<b>10317</b>	531	680	1211, 606 <sup>B</sup>	284	313	597, 299 <sup>A</sup>
<b>Model-V</b>	<b>10373</b>	456	690	1146, 573 <sup>B</sup>	290	301	591, 296 <sup>A</sup>
<b>Model-VI</b>	<b>10388</b>	474	638	1112, 556 <sup>B</sup>	322	289	611, 306 <sup>A</sup>

<sup>A,B,C</sup> Three types of diabatic energy surfaces as defined within Marcus theory in Figure 2a.

According to the standard Marcus theory,<sup>71,72</sup> we characterize polaronic properties with two relaxation energies, the sum of which is the reorganization energy (see Figure S1 and Methods section). The internal reorganization energy essentially quantifies the variation of the electronic energy due to the geometry changes when an electron is added or removed from the cluster. For simplicity we assume that the neutral and charged parabola of the diabatic energy curves have the same curvature (Figure S1). This assumes that the reorganization energies for the neutral and charged diabatic energy surfaces are identical. However, as already report on several studies,<sup>73–75</sup> the two reorganization energies and by consequence the curvature of the neutral and the charged parabola of the diabatic energy can be different (Figure 2a). The polaron binding energy ( $E_{\text{pol}}$ ) is then defined to be a half of the reorganization energy.<sup>76</sup> Generally, larger polaron binding energy reflects strong coupling of electronic system to the lattice (or electron-phonon coupling). In order to rationalize possible trends, we distinguish three cases: type A (same curve as neutral), B

(different curvature with  $\lambda_2 > \lambda_1$ ) and C (different curvature with  $\lambda_2 < \lambda_1$ ). In fact, a majority of models for an electron-charged system is type B. CsFA-MAPbI<sub>3</sub> (model III) is a unique case where an almost type A case is calculated (Table 2). The situation is different for a hole-charged system. The near-type A is observed for four cases MAPbI<sub>3</sub>, 2Cs-MAPbI<sub>3</sub> (model IV), 2FA-MAPbI<sub>3</sub> (model V) and 2(CsFA)-MAPbI<sub>3</sub> (model VI). The type C, which is not observed for the electron-charged system case, appears for the hole-charged system in three cases: CsPbI<sub>3</sub>, FA-MAPbI<sub>3</sub> (model II), and CsFA-MAPbI<sub>3</sub> (model III) clusters. Finally, the type B arises only in two cases, FAPbI<sub>3</sub> and Cs-MAPbI<sub>3</sub> (model I) clusters. It is important to note that the list of cation alloying patterns is not exhaustive. Even though there are fluctuations in binding energy and delocalization, all alloys studied have an electron polaron binding energy smaller than that of any pure material. Likewise, all alloys investigated have hole polaron binding energies smaller than MAPbI<sub>3</sub> and FAPbI<sub>3</sub>. The alloys also uniformly show consistently more charge delocalization than the pure materials.

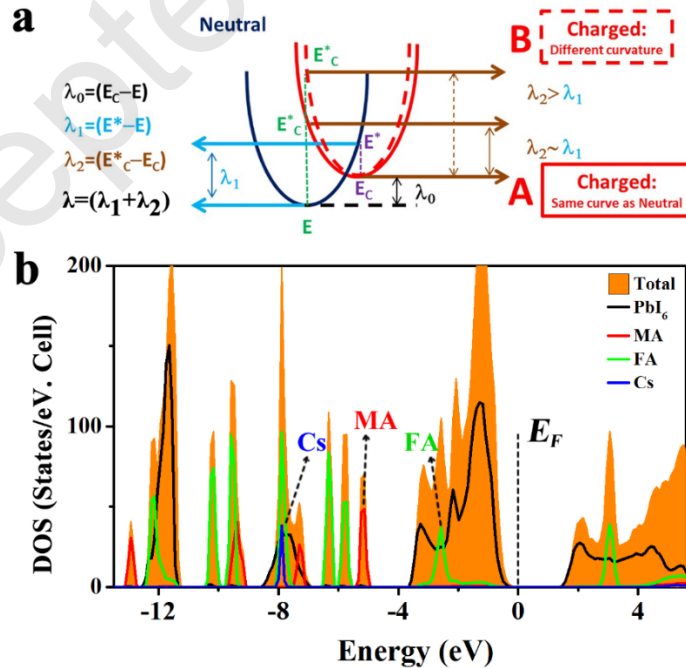


Figure 2. (a) Sketch of the three diabatic energy surfaces: Neutral (dark blue), Charged with the same curvature as Neutral (type A, red) and Charged with different from Neutral curvature (type B, dash red). Type C is not shown for clarity ( $\lambda_2 < \lambda_1$ ). (b) The computed projected DOS (pDOS) for bulk tri-halide system with a stoichiometric ratio of  $\text{Cs}_{0.063}\text{FA}_{0.688}\text{MA}_{0.25}\text{PbI}_3$ . Placement of the states of the valence band top for three cations are indicated by pink. The Fermi level is set to zero.

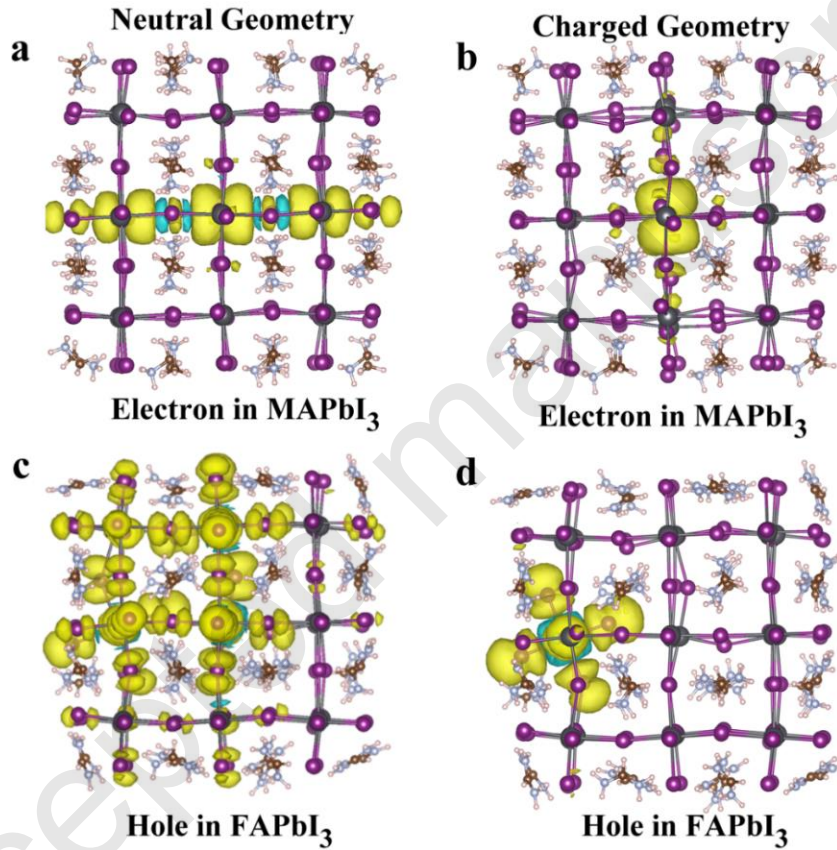


Figure 3. (a, b) The electron spin density distribution calculated using the optimal geometries of neutral and charged MAPbI<sub>3</sub> clusters, respectively. (c, d) The same as for (a,b) but for the hole spin density in FAPbI<sub>3</sub> clusters.

Figure 3a, b shows an example of spatial distribution of electron-polaron spin density in MAPbI<sub>3</sub>. While both systems have -1 charge, the left and right plots show results obtained using the neutral and negatively-charged optimal geometries, respectively. An increased spatial

localization on the right image reflects lattice relaxation accommodating an addition of extra charge (self-trapping). As expected and previously reported,<sup>69</sup> the electron  $E_{\text{pol}}$  gets smaller once the A site cation is changed from MA to Cs to FA (Table 2). This is rationalized by understanding that the MA system can stabilize a polaron via both volumetric strain and reorientation of the MA dipoles. Since both Cs and FA have vanishing or very small dipoles, only the former (local-lattice strain) mechanism remains for charge stabilization in these cases.

According to our results, Cs and FA appear to be better at mitigating hole and electron polarons formation, respectively. The small size of the Cs cation allows its free motion inside the  $\text{PbI}_6$  octahedron, which undergoes the largest JT distortion, and therefore leads to a larger electron polaron binding energy in  $\text{CsPbI}_3$  cluster compared to that in pure  $\text{FAPbI}_3$ . As discussed earlier, hole polaron formation causes uniform contraction of the surrounding lattice. In this case, having a very flexible lattice could allow for the material to “contort” itself to create a deep hole polaron. Recent experimental studies have found that FA has a near zero bulk modulus,<sup>77</sup> and we indeed find that the hole is not centrally located for the  $\text{FAPbI}_3$  cluster in the neutral geometry (Figure 3c). The hole-charged system reveals noticeable non-symmetric localization (Figure 3d) that has a binding energy almost as large as the  $\text{MAPbI}_3$  cluster (Figure S3). In addition, we analyzed the projected density of states of a bulk tri-cation perovskite  $\text{FA}_{0.688}\text{MA}_{0.25}\text{Cs}_{0.063}\text{PbI}_3$  in the tetragonal phase (Figure 2b), which has similar stoichiometric ratio to the experimental system ( $\text{FA}_{0.7}\text{MA}_{0.25}\text{Cs}_{0.05}\text{PbI}_3$ ).<sup>40</sup> Since FA states are significantly closer to the band edges, they are more likely to interact with Pb–I lattice and contribute to the overall electron-phonon coupling compared to Cs or MA. Combining this with the fact that MA generate stabilization through both lattice distortion and dipole orientation, one can rationalize why hole polarons in pure  $\text{FAPbI}_3$  are

comparatively more localized compared to pure CsPbI<sub>3</sub> and have spatial extent similar to their pure MAPbI<sub>3</sub> counterparts (see Figures S2-S4 for comparisons).

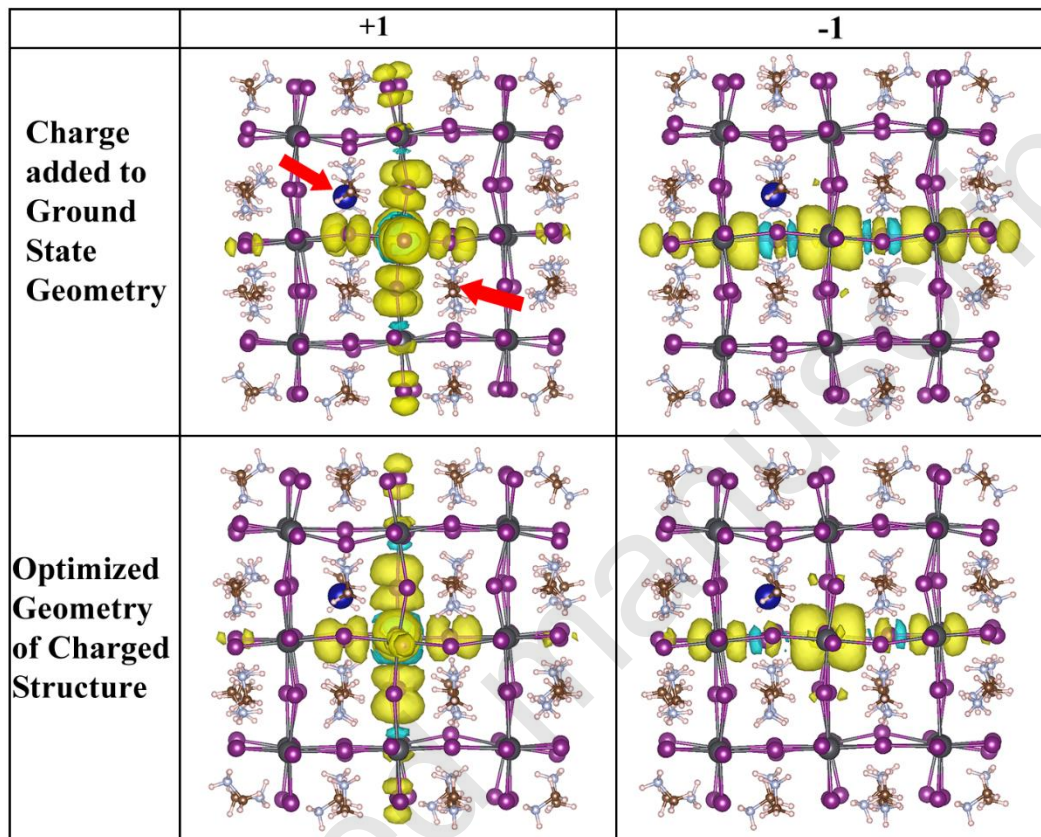


Figure 4. Calculated hole (left) and electron (right) spin density distribution of optimized neutral (top) and charged (bottom) CsFA-MAPbI<sub>3</sub> clusters (model III). The substituting Cs and FA are indicated by red arrows.

All alloyed clusters have lower electron-polaron binding energies compared to that of the pure clusters (Table 2). For example, calculated values are about half of what they are for pure MAPbI<sub>3</sub>. For hole-polarons, these alloyed systems have generally lower binding energies compared to the pure MA and FA systems with the exception of Cs-MAPbI<sub>3</sub>: the latter has polaron binding energy similar to that in the pure Cs system. Our simulations suggest that the systems with minimal electron and hole polaron binding energies are co-substituted MAPbI<sub>3</sub> (Models III and

VI) and FA-MAPbI<sub>3</sub> (Model II), respectively. The corresponding electron spin density distributions of Model-III are exemplified in Figure 4. These show slightly larger spatial extents, in good agreement with the corresponding quantities in Table 2. Spin density plots for all other alloys are shown in Figures S5–9. Overall, compared to pristine MAPbI<sub>3</sub> we observe three general concomitant trends caused by alloying: reduced lattice distortion for electrons (Table 1), decreased polaron binding energies (Table 2) and increased spatial delocalization of the polaronic spin densities. In particular, we observe that both dipolar rotation and symmetric lattice distortions become smaller upon alloying. This can be rationalized by the fact that co-substitutions with cations of different sizes lead to slightly distorted and staggered lattice. Here, for instance, the cooperative motion of the remaining MA dipoles<sup>40</sup> neighboring the substituted cells will be disrupted, thus contributing to the reduction of polaron binding energy. This in turn ensures improved delocalization of the polaron spin densities, indicating cation alloying effectively destabilizes small polarons and can potentially improve charge separation, diffusion and collection in perovskite-based optoelectronic devices supporting experimental observations.<sup>40</sup>

Our cluster models are nano-systems with a large surface to volume ratio. Even though we have been using a polarizable solvent to account for dielectric constant environment of 3D perovskites, our calculations only account for the short-range distortions associated with small polarons owing to the limited cluster size. Subsequently, we may overestimate the polaronic contributions in terms of absolute numbers. To compensate for this effect, all the systems were chosen to have approximately the same size (~2 nm) containing nearly 600 atoms and thus were sufficiently large to approximate and mimic the bulk and fractional alloy effects. Larger clusters would be computationally intractable. Despite these limitations, we expect observed trends to hold for 3D halide perovskite alloys. In addition, our calculations are static and provide just energetic



estimates for reorganization energies. The dynamics of polaronic states in alloys is a very important question, where the theoretical simulations may complement experimental ultrafast spectroscopic measurements. For example, such studies were done for  $\text{MAPI}_3$  to link exciton-polaron dynamics with lattice displacements.<sup>43</sup> Moreover, non-adiabatic molecular dynamics (NAMD) simulations<sup>78</sup> may provide additional insights into polaron dynamics. These studies in alloys are currently ongoing.

In conclusion, we perform first principle calculations to investigate how alloying the A-site cation in  $\text{APbI}_3$  halide perovskites influences structural stability, optical properties and polaron binding energy. Our cluster models show that cation alloying significantly reduces the binding energies of small polarons for both electrons and holes roughly by a factor of two compared to pure  $\text{MAPbI}_3$  and to a lesser extent compared to  $\text{CsPbI}_3$  and  $\text{FAPbI}_3$ . Observed trends are rationalized by the pre-breaking of the crystal symmetry that prevents concerted MA motion towards stabilization of a tightly bound polaron, and ultimately causes the polarons to be more spatially delocalized. The electron polarons undergo JT distortions with the central apical bonds stretching 15–30% from their neutral geometry and the equatorial bonds remaining nearly the same. The more symmetric pure materials undergo stronger JT distortions reflected and larger polaron binding energies. On the other hand, in all studied systems the Pb-I bonds in the central octahedrons of hole polarons uniformly shrink by about 5%. This difference in behavior could be utilized to determine which type of particle (electron or hole) is localized by a polaronic effect. In addition, alloying does not change significantly the band gap. Thus, our simulations show that a polaron binding energy can be tuned via Cs, FA, MA alloying, rationalizing recent experimental reports.<sup>40</sup> Overall our computational results provide detailed analysis of mechanisms of lattice

distortions due to presence of a localized charge carrier guiding experiments toward more stable halide perovskites-based materials with improved optoelectronic performance.

### **Acknowledgements**

The work at Los Alamos National Laboratory (LANL) was supported by the LANL LDRD program (A.J.N., I.A., L.Z., W.N., H.T., J.J.C., and S.T.). This work was done in part at Center for Nonlinear Studies (CNLS) and the Center for Integrated Nanotechnologies (CINT), a U.S. Department of Energy and Office of Basic Energy Sciences user facility, at LANL. This research used resources provided by the LANL Institutional Computing Program. Los Alamos National Laboratory is operated by Triad National Security, LLC, for the National Nuclear Security Administration of U.S. Department of Energy (Contract No. 89233218NCA000001). The work in France was supported by Agence Nationale pour la Recherche (TRANSHYPERO project). J.E. acknowledges financial support from the Institut Universitaire de France. A.D.M acknowledges the DOE-EERE 0001647-1544 grant for this work. A.J.N. would like to thank Mikael Kepenekian for useful insight and discussion on the set up of the calculations.

### **Supporting Information Available**

Computational details; Schematic depiction of the potential energy surfaces of the neutral and charged clusters; Hole and electron spin density distributions for pure and cation-alloyed MAPbI<sub>3</sub> clusters.

### **REFERENCES**

- (1) Manser, J. S.; Christians, J. A.; Kamat, P. V. Intriguing Optoelectronic Properties of Metal Halide Perovskites. *Chem. Rev.* **2016**, *116*, 12956–13008.
- (2) Saparov, B.; Mitzi, D. B. Organic–Inorganic Perovskites: Structural Versatility for Functional Materials Design. *Chem. Rev.* **2016**, *116*, 4558–4596.

- (3) Yamada, Y.; Nakamura, T.; Endo, M.; Wakamiya, A.; Kanemitsu, Y. Near-Band-Edge Optical Responses of Solution-Processed Organic–Inorganic Hybrid Perovskite CH<sub>3</sub>NH<sub>3</sub>PbI<sub>3</sub> on Mesoporous TiO<sub>2</sub> Electrodes. *Appl. Phys. Express* **2014**, *7*, 32302.
- (4) Chiang, C.-H.; Wu, C.-G. A Method for the Preparation of Highly Oriented MAPbI<sub>3</sub> Crystallites for High-Efficiency Perovskite Solar Cells to Achieve an 86% Fill Factor. *ACS Nano* **2018**, *12*, 10355–10364.
- (5) Wang, J.; Wang, N.; Jin, Y.; Si, J.; Tan, Z.; Du, H.; Cheng, L.; Dai, X.; Bai, S.; He, H.; et al. Interfacial Control Toward Efficient and Low-Voltage Perovskite Light-Emitting Diodes. *Adv. Mater.* **2015**, *27*, 2311–2316.
- (6) Yuan, M.; Quan, L. N.; Comin, R.; Walters, G.; Sabatini, R.; Voznyy, O.; Hoogland, S.; Zhao, Y.; Beauregard, E. M.; Kanjanaboos, P.; et al. Perovskite Energy Funnels for Efficient Light-Emitting Diodes. *Nat. Nanotechnol.* **2016**, *11*, 872–877.
- (7) Jingshan, L.; Jeong-Hyeok, I.; Mayer, M. T.; Schreier, M.; Nazeeruddin, M. K.; Nam-Gyu, P.; Tilley, S. D.; Hong Jin, F.; Gratzel, M. Water Photolysis at 12.3% Efficiency via Perovskite Photovoltaics and Earth-Abundant Catalysts. *Science (80-. )*. **2014**, *345*, 1593–1596.
- (8) Yakunin, S.; Sytnyk, M.; Kriegner, D.; Shrestha, S.; Richter, M.; Matt, G. J.; Azimi, H.; Brabec, C. J.; Stangl, J.; Kovalenko, M. V.; et al. Detection of X-Ray Photons by Solution-Processed Lead Halide Perovskites. *Nat. Photonics* **2015**, *9*, 444-U44.
- (9) Yakunin, S.; Dirin, D. N.; Shynkarenko, Y.; Morad, V.; Cherniukh, I.; Nazarenko, O.; Kreil, D.; Nauser, T.; Kovalenko, M. Detection of Gamma Photons Using Solution-Grown Single Crystals of Hybrid Lead Halide Perovskites. *Nat. Photonics* **2016**, *10*, 585–589.
- (10) Kepenekian, M.; Robles, R.; Katan, C.; Saponi, D.; Pedesseau, L.; Even, J. Rashba and

- Dresselhaus Effects in Hybrid Organic-Inorganic Perovskites: From Basics to Devices. *ACS Nano* **2015**, *9*, 11557–11567.
- (11) Muthu, C.; Nagamma, S. R.; Nair, V. C. Luminescent Hybrid Perovskite Nanoparticles as a New Platform for Selective Detection of 2,4,6-Trinitrophenol. *RSC Adv.* **2014**, *4*, 55908–55911.
- (12) Stranks, S. D.; Snaith, H. J. Metal-Halide Perovskites for Photovoltaic and Light-Emitting Devices. *Nat. Nanotechnol.* 2015, pp 391–402.
- (13) Pellet, N.; Gao, P.; Gregori, G.; Yang, T.-Y.; Nazeeruddin, M. K.; Maier, J.; Grätzel, M. Mixed-Organic-Cation Perovskite Photovoltaics for Enhanced Solar-Light Harvesting. *Angew. Chem. Int. Ed.* **2014**, *53*, 3151–3157.
- (14) Hodes, G. Perovskite-Based Solar Cells. *Science* (80-. ). **2013**, *342*, 317–318.
- (15) Niu, G.; Guo, X.; Wang, L. Review of Recent Progress in Chemical Stability of Perovskite Solar Cells. *J. Mater. Chem. A* **2015**, *3*, 8970–8980.
- (16) Li, X.; Tschumi, M.; Han, H.; Babkair, S.; Alzubaydi, A. Outdoor Performance and Stability under Elevated Temperatures and Long-Term Light Soaking of Triple-Layer Mesoporous Perovskite Photovoltaics. *Energy Technol.* **2015**, *3*, 551–555.
- (17) Grätzel, M. The Light and Shade of Perovskite Solar Cells. *Nat. Mater.* **2014**, *13*, 838–842.
- (18) Tsai, H.; Nie, W.; Blancon, J.-C.; Stoumpos, C. C.; Asadpour, R.; Harutyunyan, B.; Neukirch, A. J.; Verduzco, R.; Crochet, J. J.; Tretiak, S.; et al. High-Efficiency Two-Dimensional Ruddlesden–Popper Perovskite Solar Cells. *Nature* **2016**, *536*, 312–316.
- (19) Chen, Z.; Zhang, C.; Jiang, X.-F.; Liu, M.; Xia, R.; Shi, T.; Chen, D.; Xue, Q.; Zhao, Y.-J.; Su, S.; et al. High-Performance Color-Tunable Perovskite Light Emitting Devices through Structural Modulation from Bulk to Layered Film. *Adv. Mater.* **2017**, *29*, 1603157.

- (20) Ono, L. K.; Juarez-Perez, E. J.; Qi, Y. Progress on Perovskite Materials and Solar Cells with Mixed Cations and Halide Anions. *ACS Appl. Mater. Interfaces* **2017**, *9*, 30197–30246.
- (21) Correa-Baena, J.-P.; Abate, A.; Saliba, M.; Tress, W.; Jacobsson, T. J.; Grätzel, M.; Hagfeldt, A. The Rapid Evolution of Highly Efficient Perovskite Solar Cells. *Energy Environ. Sci.* **2017**, *10*, 710–727.
- (22) Ngo, T. T.; Suarez, I.; Antoncelli, G.; Cortizo-Lacalle, D.; Martinez-Pastor, J. P.; Mateo-Alonso, A.; Mora-Sero, I. Enhancement of the Performance of Perovskite Solar Cells, LEDs, and Optical Amplifiers by Anti-Solvent Additive Deposition. *Adv. Mater.* **2017**, *29*, 1604056.
- (23) Barker, A. J.; Sadhanala, A.; Deschler, F.; Gandini, M.; Senanayak, S. P.; Pearce, P. M.; Mosconi, E.; Pearson, A. J.; Wu, Y.; Srimath Kandada, A. R.; et al. Defect-Assisted Photoinduced Halide Segregation in Mixed-Halide Perovskite Thin Films. *ACS Energy Lett.* **2017**, *2*, 1416–1424.
- (24) Noh, J. H.; Im, S. H.; Heo, J. J.; Mandal, T. N.; Seok, S. II. Chemical Management for Colorful, Efficient, and Stable Inorganic-Organic Hybrid Nanostructured Solar Cells. *Nano Lett.* **2013**, *13*, 1764–1769.
- (25) Lee, J.-W.; Kim, D.-H.; Kim, H.-S.; Seo, S.-W.; Cho, S. M.; Park, N.-G. Formamidinium and Cesium Hybridization for Photo- and Moisture-Stable Perovskite Solar Cell. *Adv. Energy Mater.* **2015**, *5*, 1501310.
- (26) Eperon, G.; D. Stranks, S.; Menelaou, C.; B. Johnston, M.; M. Herz, L.; J. Snaith, H. Formamidinium Lead Trihalide: A Broadly Tunable Perovskite for Efficient Planar Heterojunction Solar Cells. *Energy Environ. Sci.* **2014**, *7*, 982–988.
- (27) Stoumpos, C. C.; Malliakas, C. D.; Kanatzidis, M. G. Semiconducting Tin and Lead Iodide

- Perovskites with Organic Cations: Phase Transitions, High Mobilities, and near-Infrared Photoluminescent Properties. *Inorg. Chem.* **2013**, *52*, 9019–9038.
- (28) Conings, B.; Drijkoningen, J.; Gauquelin, N.; Babayigit, A.; Haen, J. D.; Olieslaeger, L. D.; Ethirajan, A.; Verbeeck, J.; Manca, J.; Mosconi, E.; et al. Intrinsic Thermal Instability of Methylammonium Lead Trihalide Perovskite. *Adv. Energy Mater.* **2015**, *15*, 1–8.
- (29) Protesescu, L.; Yakunin, S.; Bodnarchuk, M. I.; Krieg, F.; Caputo, R.; Hendon, C. H.; Yang, R. X.; Walsh, A.; Kovalenko, M. V. Nanocrystals of Cesium Lead Halide Perovskites CsPbI<sub>3</sub>, (X = Cl, Br, and I): Novel Optoelectronic Materials Showing Bright Emission with Wide Color Gamut. *Nano Lett.* **2015**, *15*, 3692–3696.
- (30) Sutton, R. J.; Eperon, G. E.; Miranda, L.; Parrott, E. S.; Kamino, B. A.; Patel, J. B.; Hřrantner, M. T.; Johnston, M. B.; Haghighirad, A. A.; Moore, D. T.; et al. Bandgap-Tunable Cesium Lead Halide Perovskites with High Thermal Stability for Efficient Solar Cells. *Adv. Energy Mater.* **2016**, *6*, 1502458.
- (31) E. Eperon, G.; M. Patern  G.; J. Sutton, R.; Zampetti, A.; Abbas Haghighirad, A.; Cacialli, F.; J. Snaith, H. Inorganic Caesium Lead Iodide Perovskite Solar Cells. *J. Mater. Chem. A* **2015**, *3*, 19688–19695.
- (32) Yamada, K.; Nishikubo, R.; Oga, H.; Ogomi, Y.; Hayase, S.; Kanno, S.; Imamura, Y.; Hada, M.; Saeki, A. Anomalous Dielectric Behavior of a Pb/Sn Perovskite: Effect of Trapped Charges on Complex Photoconductivity. *ACS Photonics* **2018**, *5*, acsphotronics.8b00422.
- (33) Kulbak, M.; Cahen, D.; Hodes, G. How Important Is the Organic Part of Lead Halide Perovskite Photovoltaic Cells? Efficient CsPbBr<sub>3</sub> Cells. *J. Phys. Chem. Lett.* **2015**, *6*, 2452–2456.
- (34) Marronnier, A.; Roma, G.; Boyer-Richard, S.; Pedesseau, L.; Jancu, J.-M.; Bonnassieux,

- Y.; Katan, C.; Stoumpos, C. C.; Kanatzidis, M. G.; Even, J. Anharmonicity and Disorder in the Black Phases of Cesium Lead Iodide Used for Stable Inorganic Perovskite Solar Cells. *ACS Nano* **2018**, *12*, 3477–3486.
- (35) Yi, C.; Luo, J.; Meloni, S.; Boziki, A.; Ashari-Astani, N.; Grätzel, C.; M. Zakeeruddin, S.; Rühlisberger, U.; Grätzel, M. Entropic Stabilization of Mixed A-Cation ABX<sub>3</sub> Metal Halide Perovskites for High Performance Perovskite Solar Cells. *Energy Environ. Sci.* **2016**, *9*, 656–662.
- (36) McMeekin, D. P.; Sadoughi, G.; Rehman, W.; Eperon, G. E.; Saliba, M.; Hörantner, M. T.; Haghighirad, A.; Sakai, N.; Korte, L.; Rech, B.; et al. A Mixed-Cation Lead Mixed-Halide Perovskite Absorber for Tandem Solar Cells. *Science* (80-. ). **2016**, *351*, 151–155.
- (37) Yi, C.; Li, X.; Luo, J.; Zakeeruddin, S. M.; Grätzel, M. Perovskite Photovoltaics with Outstanding Performance Produced by Chemical Conversion of Bilayer Mesostructured Lead Halide/TiO<sub>2</sub> Films. *Adv. Mater.* **2016**, *28*, 2964–2970.
- (38) Saliba, M.; Matsui, T.; Domanski, K.; Seo, J.-Y.; Ummadisingu, A.; Zakeeruddin, S. M.; Correa-Baena, J.-P.; Tress, W. R.; Abate, A.; Hagfeldt, A.; et al. Incorporation of Rubidium Cations Into Perovskite Solar Cells Improves Photovoltaic Performance. *Science* (80-. ). **2016**, *354*, 206–209.
- (39) Saliba, M.; Matsui, T.; Seo, J.-Y.; Domanski, K.; Correa-Baena, J.-P.; Khaja Nazeeruddin, M.; M. Zakeeruddin, S.; Tress, W.; Abate, A.; Hagfeldt, A.; et al. Cesium-Containing Triple Cation Perovskite Solar Cells: Improved Stability, Reproducibility and High Efficiency. *Energy Environ. Sci.* **2016**, *9*, 1989–1997.
- (40) Tsai, H.; Asadpour, R.; Blancon, J.-C.; Stoumpos, C. C.; Durand, O.; Strzalka, J. W.; Chen, B.; Verduzco, R.; Ajayan, P. M.; Tretiak, S.; et al. Light-Induced Lattice Expansion Leads

- to High-Efficiency Perovskite Solar Cells. *Science* (80-. ). **2018**, *360*, 67–70.
- (41) Jeon, N. J.; Noh, J. H.; Yang, W. S.; Kim, Y. C.; Ryu, S.; Seo, J.; Seok, S. Il. Compositional Engineering of Perovskite Materials for High-Performance Solar Cells. *Nature* **2015**, *517*, 476–480.
- (42) Binek, A.; Hanusch, F. C.; Docampo, P.; Bein, T. Stabilization of the Trigonal High-Temperature Phase of Formamidinium Lead Iodide. *J. Phys. Chem. Lett.* **2015**, *6*, 1249–1253.
- (43) Nie, W.; Blancon, J.; Neukirch, A. J.; Appavoo, K.; Tsai, H.; Chhowalla, M.; Alam, M. A.; Sfeir, M. Y.; Katan, C.; Even, J.; et al. Light-Activated Photocurrent Degradation and Self-Healing in Perovskite Solar Cells. *Nat. Commun.* **2016**, *7*, 11574.
- (44) Neukirch, A. J.; Nie, W.; Blancon, J.-C.; Appavoo, K.; Tsai, H.; Sfeir, M. Y.; Katan, C.; Even, J.; Crochet, J. J.; Gupta, G.; et al. Polaron Stabilization by Cooperative Lattice and Cation Rotations in Hybrid Perovskite Materials. *Nano Lett.* **2016**, *16*, 3809–3816.
- (45) Thouin, F.; Valverde-Chávez, D. A.; Quarti, C.; Cortecchia, D.; Bargigia, I.; Beljonne, D.; Petrozza, A.; Silva, C.; Kandada, A. R. S. Phonon Coherences Reveal the Polaronic Character of Excitons in Two-Dimensional Lead Halide Perovskites. *Nat. Mater.* **2019**, *1*.
- (46) Zheng, K.; Abdellah, M.; Zhu, Q.; Kong, Q.; Jennings, G.; Kurtz, C. A.; Messing, M. E.; Niu, Y.; Gosztola, D. J.; Al-marri, M. J.; et al. Direct Experimental Evidence for Photoinduced Strong-Coupling Polarons in Organolead Halide Perovskite Nanoparticles. *J. Phys. Chem. Lett.* **2016**, *7*, 4535–4539.
- (47) Zhu, H.; Miyata, K.; Fu, Y.; Wang, J.; Joshi, P. P.; Niesner, D.; Williams, K. W.; Jin, S.; Zhu, X.-Y. Screening in Crystalline Liquids Protects Energetic Carriers in Hybrid Perovskites. *Science* (80-. ). **2016**, *353*, 1409–1413.



- (48) Miyata, K.; Atallah, T. L.; Zhu, X.-Y. Lead Halide Perovskites: Crystal-Liquid Duality, Phonon Glass Electron Crystals, and Large Polaron Formation. *Sci. Adv.* **2017**, *3*, e1701469.
- (49) Yin, J.; Li, H.; Cortecchia, D.; Soci, C.; Bredas, J. Excitonic and Polaronic Properties of 2D Hybrid Organic – Inorganic Perovskites. *ACS Energy Lett.* **2017**, *2*, 417–423.
- (50) McCall, K. M.; Stoumpos, C. C.; Kostina, S. S.; Kanatzidis, M. G.; Wessels, B. W. Strong Electron – Phonon Coupling and Self-Trapped Excitons in the Defect Halide Perovskites  $A_3M_2I_9$  ( $A = Cs, Rb$ ;  $M = Bi, Sb$ ). *Chem. Mater.* **2017**, *29*, 4129–4145.
- (51) Mahata, A.; Meggiolaro, D.; De Angelis, F. From Large to Small Polarons in Lead, Tin, and Mixed Lead–Tin Halide Perovskites. *J. Phys. Chem. Lett.* **2019**, *10*, 1790–1798.
- (52) Goldschmidt, V. M. Die Gesetze Der Krystallochemie. *Naturwissenschaften* **1926**, *14*, 477–485.
- (53) Li, C.; Soh, K. C. K.; Wu, P. Formability of  $ABO_3$  Perovskites. *J. Alloy. Compounds* **2004**, *371*, 40–48.
- (54) Li, C.; Lu, X.; Ding, W.; Feng, L.; Gao, Y.; Guo, Z. Formability of  $ABX_3$  ( $X = F, Cl, Br, I$ ) Halide Perovskites. *Acta Crystallogr. Sect. B* **2008**, *64*, 702–707.
- (55) Sun, Q.; Yin, W. Thermodynamic Stability Trend of Cubic Perovskites. *J. Am. Chem. Soc.* **2017**, *139*, 14905–14908.
- (56) Amat, A.; Mosconi, E.; Ronca, E.; Quarti, C.; Umari, P.; Nazeeruddin, M. K.; Grätzel, M.; De Angelis, F. Cation-Induced Band-Gap Tuning in Organohalide Perovskites: Interplay of Spin–Orbit Coupling and Octahedra Tilting. *Nano Lett.* **2014**, *14*, 3608–3616.
- (57) Luo, P.; Zhou, S.; Zhou, Y.; Xia, W.; Sun, L.; Cheng, J.; Xu, C.; Lu, Y. Fabrication of  $Cs_xFA_{1-x}PbI_3$  Mixed-Cation Perovskites via Gas-Phase-Assisted Compositional Modulation for Efficient and Stable Photovoltaic Devices. *ACS Appl. Mater. Interfaces*

- 2017**, 9, 42708–42716.
- (58) Pang, S.; Hu, H.; Zhang, J.; Lv, S.; Yu, Y.; Wei, F.; Qin, T.; Xu, H.; Liu, Z.; Cui, G. NH<sub>2</sub>CH=NH<sub>2</sub>PbI<sub>3</sub>: An Alternative Organolead Iodide Perovskite Sensitizer for Mesoscopic Solar Cells. *Chem. Mater.* **2014**, 26, 1485–1491.
- (59) Chen, Q.; De Marco, N.; Yang, Y. (Michael); Song, T.-B.; Chen, C.-C.; Zhao, H.; Hong, Z.; Zhou, H.; Yang, Y. Under the Spotlight: The Organic–Inorganic Hybrid Halide Perovskite for Optoelectronic Applications. *Nano Today* **2015**, 10, 355–396.
- (60) Eperon, G. E.; Stranks, S. D.; Menelaou, C.; Johnston, M. B.; Herz, L. M.; Snaith, H. J. Formamidinium Lead Trihalide: A Broadly Tunable Perovskite for Efficient Planar Heterojunction Solar Cells. *Energy Environ. Sci.* **2014**, 7, 982–988.
- (61) Pedesseau, L.; Saponi, D.; Traore, B.; Robles, R.; Fang, H.-H.; Loi, M. A.; Tsai, H.; Nie, W.; Blancon, J.-C.; Neukirch, A.; et al. Advances and Promises of Layered Halide Hybrid Perovskite Semiconductors. *ACS Nano* **2016**, 10, 9776–9786.
- (62) Niu, G.; Li, W.; Li, J.; Liang, X.; Wang, L. Enhancement of Thermal Stability for Perovskite Solar Cells through Cesium Doping. *RSC Adv.* **2017**, 7, 17473–17479.
- (63) Bella, F.; Renzi, P.; Cavallo, C.; Gerbaldi, C. Caesium for Perovskite Solar Cells: An Overview. *Chem. Eur. J.* **2018**, 24, 12183–12205.
- (64) Zuppiroli, L.; Bieber, A.; Michoud, D.; Galli, G.; Gygi, F.; Bussac, M.; Andre, J. Polaron Formation and Symmetry Breaking. *Chem. Physics* **2003**, 374, 7–12.
- (65) Holstein, T. Studies of Polaron Motion: Part II. The “Small” Polaron. *Ann. Phys. (N. Y.)* **1959**, 389, 343–389.
- (66) Frisch, M. J.; Trucks, G. W.; Schlegel, H. B.; Scuseria, G. E.; Robb, M. A.; Cheeseman, J. R.; Scalmani, G.; Barone, V.; Petersson, G. A.; Nakatsuji, H.; et al. Gaussian 16 Revision

- B.01. 2016.
- (67) Yanai, T.; Tew, D. P.; Handy, N. C. A New Hybrid Exchange–Correlation Functional Using the Coulomb-Attenuating Method (CAM-B3LYP). *Chem. Phys. Lett.* **2004**, *393*, 51–57.
- (68) Park, M.; Neukirch, A. J.; Reyes-Lillo, S. E.; Lai, M.; Ellis, S. R.; Dietze, D.; Neaton, J. B.; Yang, P.; Tretiak, S.; Mathies, R. A. Excited-State Vibrational Dynamics Toward the Polaron in Methylammonium Lead Iodide Perovskite. *Nat. Commun.* **2018**, *9*, 2525.
- (69) Neukirch, A. J.; Abate, I.; Iwnetim, I.; Zhou, Li.; Nie, W.; Hsinhan, T.; Pedesseau, L.; Even, J.; Crochet, J. J.; Mohite, A. J.; Katan, C.; et al. Geometry Distortion and Small Polaron Binding Energy Changes with Ionic Substitution in Halide Perovskites. *J. Phys. Chem. Lett.* **2018**, *9*, 7130–7136.
- (70) Varignon, J.; Bristowe, N. C.; Ghosez, P. Electric Field Control of Jahn-Teller Distortions in Bulk Perovskites. *Phys. Rev. Lett.* **2016**, *057602*, 1–6.
- (71) Marcus, R. A. On the Theory of Oxidation-Reduction Reactions Involving Electron Transfer. II. Applications to Data on the Rates of Isotopic Exchange Reactions. *J. Chem. Phys.* **1957**, *26*, 867–871.
- (72) Marcus, R. A. Electron Transfer Reactions in Chemistry: Theory and Experiment (Nobel Lecture). *Rev. Mod. Phys.* **1993**, *32*, 1111–1121.
- (73) Yang, D. Y.; Cukier, R. I. The Transition from Nonadiabatic to Solvent Controlled Adiabatic Electron Transfer: Solvent Dynamical Effects in the Inverted Regime. *J. Chem. Phys.* **1989**, *91*, 281–292.
- (74) Tang, J. Electron-Transfer Reactions Involving Non-Linear Spin-Boson Interactions. *Chem. Phys.* **1994**, *188*, 143–160.
- (75) Denk, C.; Morillo, M.; Sánchez-Burgos, F.; Sánchez, A. Reorganization Energies for

- Charge Transfer Reactions in Binary Mixtures of Dipolar Hard Sphere Solvents: A Monte Carlo Study. *J. Chem. Phys.* **1998**, *110*, 473–483.
- (76) Coropceanu, V.; Cornil, J.; da Silva Filho, D. A.; Olivier, Y.; Silbey, R.; Brédas, J.-L. Charge Transport in Organic Semiconductors. *Chem. Rev.* **2007**, *107*, 926–952.
- (77) Ferreira, A. C.; Léotoublon, A.; Paofai, S.; Raymond, S.; Ecolivet, C.; Rufflé B.; Cordier, S.; Katan, C.; Saidaminov, M. I.; Zhumekenov, A. A.; et al. Elastic Softness of Hybrid Lead Halide Perovskites. *Phys. Rev. Lett.* **2018**, *121*, 1–6.
- (78) Yin, J.; Maity, P.; Bastiani, M. De; Dursun, I.; Bakr, O. M.; Brédas, J.-L.; Mohammed, O. F. Molecular Behavior of Zero-Dimensional Perovskites. *Sci. Adv.* **2017**, *3*, e1701793.